

# Nonequilibrium Phase Transitions in Repulsive Binary Mixtures

Pedro Antonio Santos-Flórez<sup>1</sup> and Maurice de Koning<sup>1,2,\*</sup>

<sup>1</sup>*Instituto de Física "Gleb Wataghin", Universidade Estadual de Campinas,  
UNICAMP, 13083-859, Campinas, São Paulo, Brazil*

<sup>2</sup>*Center for Computing in Engineering & Sciences, Universidade Estadual de Campinas,  
UNICAMP, 13083-861, Campinas, São Paulo, Brazil*

(Dated: December 21, 2024)

We consider rapid cooling processes in classical, 3-dimensional, purely repulsive binary mixtures in which an initial infinite-temperature configuration is instantly quenched to zero temperature. It is found that such systems display both kinds of possible continuous nonequilibrium transition, characterized by either a conserved or non-conserved order parameter. The type of transition that is observed can be controlled by tuning the interactions between unlike particles, with strong inter-species repulsion leading to chemical ordering in terms of an unmixing process, whereas weak repulsion gives rise to spontaneous crystallization, maintaining chemical homogeneity. In contrast to common first-order equilibrium freezing transitions, this nonequilibrium crystallization phenomenon is continuous in nature, being barrierless and producing grain-size distributions that display scale-invariant features. Furthermore, the results suggest that the dual-type transition behavior is universal for repulsive pair interaction potential-energy functions in general, with the propensity for the continuous freezing transition being related to their behavior in the neighborhood of zero separation.

Classical systems described by repulsive pair potentials have been the subject of intense investigation for over five decades [1–31]. Not in the least due to their role as effective descriptions for interactions in soft-condensed-matter systems [32–42], substantial effort has been directed towards elucidating the equilibrium phase behavior of such models, considering both single-component samples as well as multi-component mixtures [17–31]. Nonequilibrium phenomena, on the other hand, have received much less attention, despite their key role in self-organization phenomena in such systems [43–53]. Indeed, one of the challenges in soft-matter materials design concerns the ability to adjust the effective interaction parameters so as to control the self-organization process and achieve desired self-assembled structures [53].

In this context, processes that display spontaneous development of structure from an initially disordered, far-from-equilibrium state are of particular interest [43, 52, 53]. A typical example are so-called ageing phenomena [56] in which a system initially at equilibrium in a high-temperature state is rapidly quenched to low temperature. Due to the rapid pace of cooling, the initial high-temperature phase becomes unstable and will spontaneously decay into some low-temperature state. When considering mixtures, this decay can occur by means of two different types of continuous nonequilibrium phase transition, depending on whether the involved order parameter is conserved or non-conserved, and which, on the continuum level, are described by the celebrated Allen-Cahn and Cahn-Hilliard equations, respectively [54, 56]. The prototypical example of the first kind are unmixing transitions in which the order parameter is related to the fixed chemical composition and the final low-temperature state is characterized by chemical ordering through phase separation. In the second type, on the other hand, the

final state is typified by the development of structural order, as described by a non-conserved order parameter related to, for instance, quantities such as crystal symmetry and/or orientation [54, 56]. However, while unmixing transitions are quite common for the class of repulsive pair potentials [41, 57, 58], the occurrence of the second type of transition is not. In fact, as far as model systems are concerned, to the best of our knowledge such structural ordering phenomena have so far only been observed for discrete spin systems such as the Ising model [56], while there have been no reports for systems characterized by continuous interactions. Above all, to date there are no known model systems that can display both types of transition as a function of boundary conditions and/or model parameters.

Here we show that 3-dimensional binary mixtures described by purely repulsive pairwise interactions display both kinds of nonequilibrium transition and that the observed type can be controlled by tuning the interactions between unlike particles. While strong inter-species repulsion gives rise to chemical ordering through unmixing, weak values lead to a spontaneous development of structural order, forming a polycrystalline solid of uniform chemical composition. Unlike the common equilibrium first-order freezing transitions, however, this nonequilibrium crystallization process is continuous in nature in that it is barrierless and gives rise to grain-size distributions that display scale-invariant characteristics. Furthermore, the results suggest that the dual-type nonequilibrium transition behavior is universal for pairwise repulsive potential-energy functions in general and that the propensity of the continuous structural ordering transition is related to their behavior in the neighborhood of zero separation.

Since the main focus is on the nature of the final state

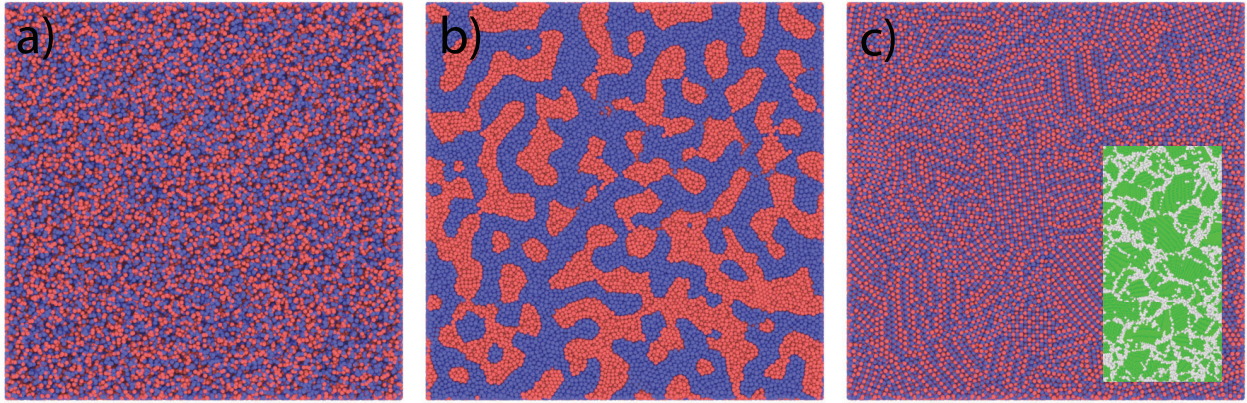


Figure 1. (Color online) Typical configurations containing  $N = 10^7$  particles, with the distinct species shown in blue and red, respectively, as obtained from the CG quench protocol for the binary UF model for two different values for the inter-species interaction energy scale. a) Random initial configuration. b) Phase-separating system for strong inter-species repulsion. c) Spontaneous ordering into a rock-salt (B1) type polycrystal of uniform composition. Inset displays part of the grain structure, with the green and white particles representing those in the B1 structure and in the disordered surroundings of the grain boundaries, respectively, as determined using the *Ovito* package [59, 60].

of the cooling processes, our results are based on simulations in which an initial infinite-temperature state is instantly quenched to zero temperature. Because the quench is infinitely rapid, the system has no time to explore the potential-energy landscape (PEL) and is instantaneously driven to the local minimum closest to the initial configuration, also known as its inherent structure [61–63]. This quench process is implemented computationally in the following way. First, for a specified particle density, we construct a cubic, periodic simulation cell with a volume  $V$  that corresponds to a given total particle number  $N$ . Subsequently, the system is initialized by randomly placing the  $N$  particles in the cell, giving rise to a structureless, uniform position distribution that represents an infinite-temperature state. Then, to locate the corresponding inherent structure, a conjugate-gradient (CG) minimization is invoked. For each set of interaction properties and particle densities this procedure is repeated several times using different random initial conditions. All the CG calculations have been performed using the Polak-Ribiere version of the CG algorithm as implemented in the LAMMPS package [64], which is among the most efficient local minimization algorithms for functions of many variables [65].

As a first case we consider a binary mixture with inter-particle interactions described by the Uhlenbeck-Ford (UF) model [66–69], which is characterized by a logarithmic divergence at zero separation and belongs to the class of so-called ultrasoft potentials [36]. Specifically, the UF model is defined by the potential-energy function  $u(r_{ij}) = -\epsilon_{ij} \ln(1 - e^{-r_{ij}^2/\sigma_{ij}^2})$ , where  $\epsilon_{ij}$  and  $\sigma_{ij}$  are energy and length scales associated with the interactions between particles  $i$  and  $j$ , and  $r_{ij}$  is the distance between them. We fix the energy scales of the interactions be-

tween particles of the same species to be  $\epsilon_{AA} = 100\epsilon$  and  $\epsilon_{BB} = 200\epsilon$ , respectively, whereas the energy scale  $\epsilon_{AB}$  for interactions between  $A$  and  $B$  particles is variable. The length scale is chosen to be the same for all interaction types, i.e.,  $\sigma_{AA} = \sigma_{BB} = \sigma_{AB} = \sigma$  and the cut-off for the interaction calculation is set at  $r_c = 4\sigma$ . Species  $A$  and  $B$  are present in equal proportions for all cases, including for the other interaction models discussed below.

Fig. 1 displays typical configurations obtained for the UF mixture containing  $10^7$  particles at a reduced particle density  $\rho^* \equiv N\sigma^3/V = 1$ . Fig. 1a) depicts a typical random initial condition that is disordered both chemically and structurally. Figs. 1b) and c) then show snapshots obtained from the subsequent CG minimizations for two different values of the inter-species interaction parameter,  $\epsilon_{AB}$ .

Fig. 1b) portrays a case of strong inter-species repulsion at  $\epsilon_{AB} = 175\epsilon$ . Under these conditions the system is unstable with respect to composition fluctuations [70] and undergoes a chemical ordering transition by which the two species unmix. This transformation corresponds to the first type of nonequilibrium transition discussed above, involving a conserved order parameter. Indeed, the depicted structure strongly resembles the typical patterns of spinodal decomposition often seen for phase separation [54]. Note, however, that the structure depicted in Fig. 1b) has not yet fully converged to the completely unmixed inherent structure. This is because the computational cost to reach a fully unmixed state is prohibitively large for the system size considered here, even for efficient minimizers such as CG. For smaller system sizes, however ( $N \sim 10^5 - 10^6$ ), complete unmixing is attained within reasonable computational limits.

For a weak inter-species interaction at  $\epsilon_{AB} = 20\epsilon$ , the

instability is fundamentally different. In this case the CG minimization rapidly converges to the inherent structure displayed in Fig. 1c), which remains uniform with respect to chemical composition but has spontaneously developed structural order. In particular, it features a polycrystalline morphology composed of grains with the rock-salt (B1) structure, which consists of two interpenetrating fcc lattices, each occupied by either  $A$  or  $B$ . Interestingly, the nature of this crystallization process is fundamentally different from the usual first-order character of equilibrium freezing phenomena. The nonequilibrium crystallization transition observed here is continuous in nature. First, there is no energy barrier between the structureless initial configuration and the final polycrystalline structure since they are connected by a CG sequence that always moves downhill on the PES [65]. This is the main difference compared to first-order transitions, for which initial and final configurations are separated by an energy barrier that cannot be surmounted using local minimization techniques such as CG. Secondly, the grain-size distribution of the polycrystalline structure displays the same scale-invariant features characteristic for equilibrium continuous phase transitions such as, for instance, in the cluster-size distribution of the percolation transition [71].

To demonstrate the latter, we employ the recently developed grain-segmentation algorithm (GSA) in Ovito [59, 60] to identify individual grains and determine their sizes in terms of particle numbers for the final configuration from a CG minimization with  $\epsilon_{AB} = 20\epsilon$ . Fig. 2 shows a log-log rank-size representation [71, 72] of the grain-size distribution in which the rank of each grain in terms of its size is plotted as a function of grain size, such that the largest and smallest grains are ranked first and last, respectively. For this particular purpose, to enhance the grain statistics, we have carried out a single quench simulation on a  $10^8$  particle cell, with its inherent structure containing more than  $4 \times 10^4$  crystallites with sizes ranging between 100 and  $\sim 6 \times 10^4$  particles. The size-rank graph in Fig. 2 clearly displays a linear regime for grain sizes  $\geq 10^4$  particles. This suggests that, asymptotically, the distribution for the grain size  $k$  follows a power law of the form  $p(k) \sim k^{-\alpha}$  (with  $\alpha = 3.64 \pm 0.02$  in this case) and displays scale invariance.

In all of the cases shown above, the results are independent of the random initial condition, displaying the same unmixing and crystallization transitions for different random-number seeds. Accordingly, for a given particle-number density, the type of transition that occurs is determined by the magnitude of the interspecies interaction strength  $\epsilon_{AB}$  only. To further analyze its role we carry out a series of quench CG simulations for a set of  $\epsilon_{AB}$ -values between 0 and  $200\epsilon$ , employing cells containing of the order of  $10^3 - 10^4$  particles. In addition, we also investigate the possible influence of the particle-number density by considering a range of  $\rho^*$ -values for each  $\epsilon_{AB}$ .

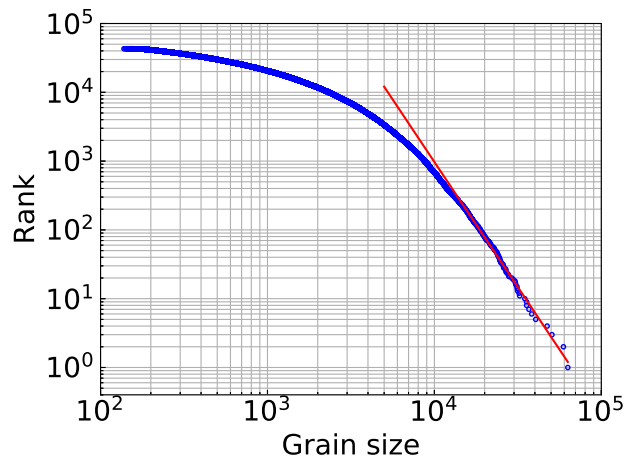


Figure 2. (Color online) Log-log graph of rank-size representation of the grain size distribution for cell containing  $10^8$  particles as obtained using the grain-segmentation tool of the Ovito package [59, 60], plotting the rank of each grain in terms of its size as a function of grain size, such that the largest and smallest grains are ranked first and last, respectively. Blue circles depict results data points of individual grains. Red line represents a guide to the eye, obtained by a linear fit to the data for the 200 largest grains, which amount to grain sizes greater than  $\sim 1.5 \times 10^4$  particles.

To automate the detection of the phase transitions we monitor the displacements of the particles during each quench simulation, comparing their positions in the initially structureless state to those at the end of the CG minimization procedure. Fig. 3a) displays a density plot of the mean particle displacements (MPD) for the UF system as a function of  $\epsilon_{AB}$  and  $\rho^*$ , expressed in units of the particle-density length scale  $d \equiv \rho^{*-1/3}$ . It displays three well-defined regimes, characterized by distinct values for the mean particle displacement. The yellow band on the left corresponds to values of the order of  $\sim 2d$  and signals the instability of the random initial configuration that leads to its decay into the self-similar rock-salt structure through the continuous ordering transition. The mostly blue band on the right corresponds to the instability that gives rise to the unmixing transition in which particles move over significantly larger distances. Finally, in the orange-colored areas the displacements are less than the average particle separation, meaning that the initial configurations are metastable, i.e., they are “close” to their corresponding local minima, which retain their chemically uniform and structurally disordered character. A further notable characteristic is that the identification of these 3 groups involves  $\epsilon_{AB}$  only, being essentially independent of  $\rho^*$ , except for very low values for which the distances between the particles become large and the interactions between them weak. This implies that the inherent structures associated with high-temperature configurations are invariant with respect to uniform volume

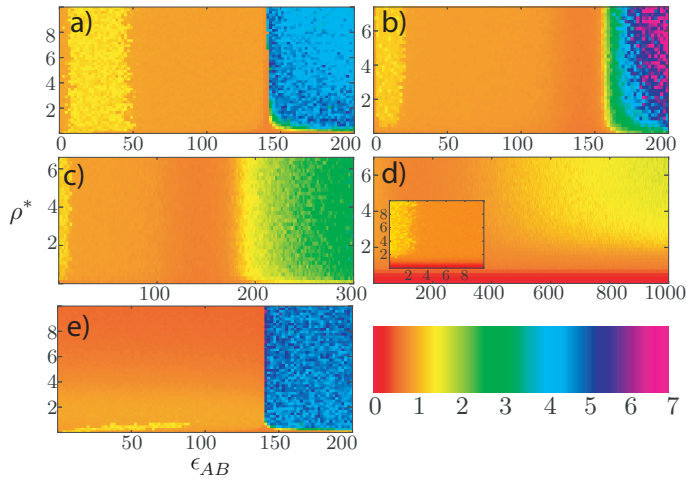


Figure 3. (Color online) Density plots of mean particle displacement in units of the mean interparticle distance  $d \equiv \rho^*^{-1/3}$  during CG quench as a function of the interaction energy scale  $\epsilon_{AB}$  and the reduced density  $\rho^*$  for the UF model (a), the IPL4 (b), IPL6 (c), WCA (d) and GC (e) potentials. Inset in (d) shows zoom into region with  $\epsilon_{AB} < 10\epsilon$ . Colors defined in the color bar distinguish between different displacement magnitudes.

scaling [62].

Interpreted from the perspective of the PEL formalism [62], the above findings imply that, for the considered binary UF model, the topography of the inherent structures for uniformly sampled configurations undergoes abrupt transitions as a function of the interspecies interaction intensity. At  $\epsilon_{AB} \simeq 5$  and 50 there is an abrupt transition between chemically uniform, amorphous inherent structures and local minima that display polycrystalline structural order at a homogeneous composition. When reaching  $\epsilon_{AB} \simeq 150$ , on the other hand, there is a second kind of transition, with the nature of the inherent structures changing from chemically uniform and structurally ordered to compositionally unmixed without long-range structural order.

Another important finding is that the observed phenomena are not limited to the binary UF system but seem to be universal for repulsive interaction potential-energy functions in general. This is illustrated in Figs. 3 b-e), which depict density plots of the mean particle distance for the inverse fourth-power law (IPL4), the inverse sixth-power law (IPL6), the Weeks-Chandler-Andersen (WCA) and the Gaussian core (GC) models [70], respectively. For all these systems the same 3 regimes can be identified, observing unmixing for large values for  $\epsilon_{AB}$ , continuous structural ordering to chemically uniform, rock-salt-type polycrystals for weak interspecies interactions and chemically/structurally amorphous configurations in between.

A particularly interesting issue in this context concerns the relation between the continuous structural ordering regime and the functional form of the repulsive interac-

tion. Specifically, the shape and the extent of the continuous ordering region in Fig. 3 is seen to correlate with the rate at which the potential-energy function diverges at the origin. Along the sequence shown in Fig. 3 a) to d), in which the divergence changes from slow (logarithmic) to fast ( $r^{-12}$ ), the range of energy scales  $\epsilon_{AB}$  for which continuous crystallization occurs reduces systematically. Indeed, the role of the behavior of the pair potential at the origin in the ordering transition becomes even more evident when considering the GC force field, which does not diverge at all, tending to a constant value and zero derivative at the origin. [70] As shown in Fig. 3 e), the ordering transition to the rock-salt polycrystal structure in this case is restricted to a very narrow region in the  $\epsilon_{AB}-\rho^*$  plane, disappearing altogether for densities above  $\sim 0.8$ .

In conclusion, we have considered the nonequilibrium behavior of classical, 3-dimensional binary mixtures of particles interacting through purely repulsive forces during processes in which an infinite-temperature initial structure is rapidly quenched to zero temperature. We find that such systems display both possible types of second-order nonequilibrium phase transition, characterized by either a conserved or non-conserved order parameter. The observed type of transition can be controlled by tuning the interactions between unlike particles, with strong inter-species repulsion giving rise to unmixing, whereas weak interactions lead to a spontaneous development of structural order, forming a rock-salt-type polycrystalline solid of uniform composition. Unlike common first-order equilibrium freezing transitions, however, this crystallization process is continuous in nature, being barrierless and displaying scale-invariant features in the grain-size distributions. Furthermore, the findings suggest that the dual-type transition behavior is universal for repulsive pair interaction potential-energy functions in general, with the propensity for the continuous freezing transition being related to their behavior in the neighborhood of zero separation.

We gratefully acknowledge support from the Brazilian agencies CNPq, Capes, Fapesp 2016/23891-6 and the Center for Computing in Engineering & Sciences - Fapesp/Cepid no. 2013/08293-7. Part of the calculations were performed at CCJDR-IFGW-UNICAMP. The authors acknowledge the National Laboratory for Scientific Computing (LNCC/MCTI, Brazil) for providing HPC resources of the SDumont supercomputer, which have contributed to the research results reported in this paper. URL: <http://sdumont.lncc.br>. We thank Alexander Stukowski and Peter Larsen for their assistance with Ovito's grain segmentation algorithm.

\* dekonig@if.unicamp.br

- [1] F. H. Stillinger and E. Helfand, *J. Chem. Phys.* **41**, 2495 (1964).
- [2] E. Helfand and F. H. Stillinger, *J. Chem. Phys.* **49**, 1232 (1968).
- [3] A. Baram, *J. Phys. A* **16**, L19 (1983).
- [4] A. Baram and J. S. Rowlinson, *J. Phys. A* **23**, L399 (1990).
- [5] A. Baram and J. S. Rowlinson, *Mol. Phys.* **74**, 707 (1991).
- [6] A. Baram, M. Maddox, and J. S. Rowlinson, *Mol. Phys.* **76**, 1093 (1992).
- [7] A. Baram, M. Maddox, and J. S. Rowlinson, *Mol. Phys.* **79**, 589 (1993).
- [8] M. Dijkstra and R. van Roij, *J. Phys.: Condens. Matter* **10**, 1219 (1998).
- [9] A. Lang, C. N. Likos, M. Watzlawek, and H. Löwen, *J. Phys.: Condens. Matter* **12**, 5087 (2000).
- [10] A. A. Louis, P. G. Bolhuis, and J. P. Hansen, *Phys. Rev. E* **62**, 7961 (2000).
- [11] R. J. Speedy, *J. Phys.: Condens. Matter* **15**, S1243 (2003).
- [12] G. Cinacchi, Y. Martínez-Ratón, L. Mederos, G. Navascués, A. Tani, and E. Velasco, *J. Chem. Phys.* **127**, 214501 (2007).
- [13] M. A. Glaser, G. M. Grason, R. D. Kamien, A. Košmrlj, C. D. Santangelo, and P. Ziherl, *EPL* **78**, 46004 (2007).
- [14] F. Saija, S. Prestipino, and G. Malescio, *Phys. Rev. E* **80**, 031502 (2009).
- [15] L. Berthier, E. Flenner, H. Jacquin, and G. Szamel, *Phys. Rev. E* **81**, 031505 (2010).
- [16] M. Schmiedeberg, T. K. Haxton, S. R. Nagel, and A. J. Liu, *EPL* **96**, 36010 (2011).
- [17] J. Russo and H. Tanaka, *Soft Matter* **8**, 4206 (2012).
- [18] A. Travesset, *Proc Natl Acad Sci USA* (2015).
- [19] N. Horst and A. Travesset, *J. Chem. Phys.* **144**, 014502 (2016).
- [20] F. H. Stillinger, *J. Chem. Phys.* **65**, 3968 (1976).
- [21] P. Hansen, J., D. Goulding, and R. van Roij, *J. Phys. IV France* **10**, Pr5 (2000).
- [22] S. Prestipino, F. Saija, and P. V. Giaquinta, *J. Chem. Phys.* **123**, 144110 (2005).
- [23] S. Prestipino, F. Saija, and P. V. Giaquinta, *Phys. Rev. E* **71**, 050102(R) (2005).
- [24] G. Malescio and G. Pellicane, *Nat. Mater.* **2**, 97 (2003).
- [25] B. M. Mladek, D. Gottwald, G. Kahl, M. Neumann, and C. N. Likos, *Phys. Rev. Lett.* **96**, 045701 (2006).
- [26] C. N. Likos, B. M. Mladek, D. Gottwald, and G. Kahl, *J. Chem. Phys.* **126**, 224502 (2007).
- [27] C. N. Likos, B. M. Mladek, A. J. Moreno, D. Gottwald, and G. Kahl, *Comput. Phys. Commun.* **179**, 71 (2008).
- [28] S. D. Overduin and C. N. Likos, *EPL* **85**, 26003 (2009).
- [29] A. J. Archer, C. N. Likos, and R. Evans, *J. Phys.: Condens. Matter* **16**, L297 (2004).
- [30] H. Shin, G. M. Grason, and C. D. Santangelo, *Soft Matter* **5**, 3629 (2009).
- [31] L. A. Shall and S. A. Egorov, *J. Chem. Phys.* **132**, 184504 (2010).
- [32] C. N. Likos, H. Löwen, M. Watzlawek, B. Abbas, O. Jucknischke, J. Allgaier, and D. Richter, *Phys. Rev. Lett.* **80**, 4450 (1998).
- [33] M. Watzlawek, C. N. Likos, and H. Löwen, *Phys. Rev. Lett.* **82**, 5289 (1999).
- [34] C. von Ferber, A. Jusufi, M. Watzlawek, C. N. Likos, and H. Löwen, *Phys. Rev. E* **62**, 6949 (2000).
- [35] C. N. Likos, *Phys. Rep.* **348**, 267 (2001).
- [36] C. N. Likos, N. Hoffmann, H. Löwen, and A. A. Louis, *J. Phys.: Condens. Matter* **14**, 7681 (2002).
- [37] C. N. Likos, *Soft Matter* **2**, 478 (2006).
- [38] C. Mayer, E. Zaccarelli, E. Stiakakis, C. N. Likos, F. Sciortino, A. Munam, M. Gauthier, N. Hadjichristidis, H. Iatrou, P. Tartaglia, H. Lowen, and D. Vlassopoulos, *Nat. Mater.* **7**, 780 (2008).
- [39] B. M. Mladek, G. Kahl, and C. N. Likos, *Phys. Rev. Lett.* **100**, 028301 (2008).
- [40] C. Mayer, F. Sciortino, C. N. Likos, P. Tartaglia, H. Löwen, and E. Zaccarelli, *Macromolecules* **42**, 423 (2009).
- [41] M. Camargo and C. N. Likos, *Mol. Phys.* **109**, 1121 (2011).
- [42] A. Nikoubashman, N. A. Mahynski, B. Capone, A. Z. Panagiotopoulos, and C. N. Likos, *J. Chem. Phys.* **143**, 243108 (2015).
- [43] G. Nicolis and I. Prigogine, *Self-Organization in Nonequilibrium Systems: From Dissipative Structures to Order Through Fluctuations* (Wiley, 1977).
- [44] T. A. Witten, *Rev. Mod. Phys.* **71**, S367 (1999).
- [45] R. L. Marson, C. L. Phillips, J. A. Anderson, and S. C. Glotzer, *Nano Lett.* **14**, 2071 (2014).
- [46] A. M. Kalsin, M. Fialkowski, M. Paszewski, S. K. Smoukov, K. J. M. Bishop, and B. A. Grzybowski, *Science* **312**, 420 (2006).
- [47] W. L. Miller and A. Cacciuto, *Phys. Rev. E* **80**, 021404 (2009).
- [48] X. Ye, C. Zhu, P. Ercius, S. N. Raja, B. He, M. R. Jones, M. R. Hauwiller, Y. Liu, T. Xu, and A. P. Alivisatos, *Nature Communications* **6**, 10052 (2015).
- [49] A. Kumar and V. Molinero, *J. Phys. Chem. Lett.* **8**, 5053 (2017).
- [50] X. Ye, J. Chen, and C. B. Murray, *J. Am. Chem. Soc.* **133**, 2613 (2011).
- [51] R. J. Macfarlane, B. Lee, M. R. Jones, N. Harris, G. C. Schatz, and C. A. Mirkin, *Science* **334**, 204 (2011).
- [52] C. Knorowski, S. Burleigh, and A. Travesset, *Phys. Rev. Lett.* **106**, 215501 (2011).
- [53] C. Knorowski and A. Travesset, *Curr. Opin. Solid State Mater. Sci.* **15**, 262 (2011).
- [54] R. Balluffi, S. Allen, W. Carter, and R. Kemper, *Kinetics Of Materials* (J. Wiley & Sons, 2005) pp. –.
- [55] H. Hinrichsen, *Fundamental Problems in Statistical Physics*, *Physica A* **369**, 1 (2006).
- [56] M. Henkel and M. Pleimling, *Non-Equilibrium Phase Transitions: Volume 2: Ageing and Dynamical Scaling Far from Equilibrium* (Springer Netherlands, 2011).
- [57] A. J. Archer and R. Evans, *Phys. Rev. E* **64**, 041501 (2001).
- [58] S. Kambayashi and Y. Hiwatari, *Phys. Rev. A* **46**, 1014 (1992).
- [59] A. Stukowski, *Model. Simul. Mater. Sci. Eng.* **18**, 015012 (2010).
- [60] P. M. Larsen, S. Schmidt, and J. Schiötz, *Modell. Simul. Mater. Sci. Eng.* **24**, 055007 (2016).
- [61] F. H. Stillinger, *Science* **267**, 1935 (1995).
- [62] F. Stillinger, *Energy Landscapes, Inherent Structures, and Condensed-Matter Phenomena* (Princeton University Press, 2015).
- [63] D. J. Wales, *Energy Landscapes: Applications to Clusters, Biomolecules and Glasses* (Cambridge University Press, 2003).
- [64] S. Plimpton, *J. Comput. Phys.* **117**, 1 (1995).

- [65] W. Press, S. Teukolsky, W. Vetterling, and B. Flannery, *Numerical Recipes 3rd Edition: The Art of Scientific Computing* (Cambridge University Press, 2007).
- [66] G. Uhlenbeck and G. Ford, Studies in statistical mechanics, in *Series in physics*, v. 1, edited by J. de Boer and G. Uhlenbeck (North-Holland Publishing Company, 1962) Chap. The development of linear graphs with applications to the theory of the virial development of the properties of gases, p. 182.
- [67] R. Paula Leite, R. Freitas, R. Azevedo, and M. de Koning, J. Chem. Phys. **145**, 194101 (2016).
- [68] R. Paula Leite, P. A. Santos-Flórez, and M. de Koning, Phys. Rev. E **96**, 032115 (2017).
- [69] R. Paula Leite and M. de Koning, Comput. Mater. Sci. **159**, 316 (2019).
- [70] For further details, see Supplemental Material.
- [71] M. Newman, Contemp. Phys. **46**, 323 (2005).
- [72] A. Clauset, C. Shalizi, and M. Newman, SIAM Rev. **51**, 661 (2009).

# Supplemental Material for “Nonequilibrium Phase Transitions in Repulsive Binary Mixtures”

Pedro Antonio Santos-Flórez<sup>1</sup> and Maurice de Koning<sup>1,2,\*</sup>

<sup>1</sup>*Instituto de Física “Gleb Wataghin”, Universidade Estadual de Campinas, UNICAMP, 13083-859, Campinas, São Paulo, Brazil*

<sup>2</sup>*Center for Computing in Engineering & Sciences, Universidade Estadual de Campinas, UNICAMP, 13083-861, Campinas, São Paulo, Brazil*

(Dated: December 21, 2024)

## I. INTERACTIONS MODELS

We consider the set of purely repulsive interaction models detailed below. In all cases,  $\epsilon_{ij}$  and  $\sigma_{ij}$  are energy and length scales associated with the interactions between particles  $i$  and  $j$ , and  $r_{ij}$  is the distance between them. In all simulations we fix the energy scales of the interactions between particles of the same species to be  $\epsilon_{AA} = 100\epsilon$  and  $\epsilon_{BB} = 200\epsilon$ , respectively, whereas the energy scale  $\epsilon_{AB}$  for interactions between  $A$  and  $B$  is variable. The length scale is chosen to be the same for all interaction types, i.e.,  $\sigma_{AA} = \sigma_{BB} = \sigma_{AB} = \sigma$ .

### A. Uhlenbeck-Ford

The interactions described by the purely repulsive Uhlenbeck-Ford (UF) model<sup>1-4</sup> are characterized by a logarithmic divergence at zero separation and belong to the class of so-called ultrasoft potentials<sup>5</sup>, which have been shown to be useful in the description of the effective interactions between star-polymer particles<sup>6-9</sup>. Specifically, the UF model is defined by the potential-energy function

$$u(r_{ij}) = -\epsilon_{ij} \ln(1 - e^{-r_{ij}^2/\sigma_{ij}^2}). \quad (1)$$

The cut-off for the interaction calculation is set at  $r_c = 4\sigma$ .

### B. Inverse fourth-power and sixth-power laws

The potential-energy functions describing the inverse fourth (IPL4) and sixth-power (IPL6) laws<sup>10</sup> are given by

$$u(r_{ij}) = \epsilon_{ij} \left( \frac{\sigma_{ij}}{r_{ij}} \right)^n, \quad (2)$$

with the cut-offs for the interaction calculation set at  $r_c = 6\sigma$  and  $r_c = 4\sigma$ , respectively, for the IPL4 and IPL6 models.

## C. Weeks-Chandler-Andersen

The Weeks-Chandler-Anderson (WCA) model<sup>11</sup> is defined by the repulsive part of the Lennard-Jones (LJ) potential energy function, shifting the LJ function such that the minimum value corresponds to zero, and truncating it for distances beyond that of its minimum at  $r = 2^{1/6}\sigma$ . For the binary mixture, the WCA force field is defined as

$$u(r_{ij}) = \begin{cases} 4\epsilon_{ij} \left[ \left( \frac{\sigma_{ij}}{r_{ij}} \right)^{12} - \left( \frac{\sigma_{ij}}{r_{ij}} \right)^6 \right] + \epsilon_{ij}, & \text{if } r \leq 2^{1/6} \sigma_{ij} \\ 0, & \text{otherwise.} \end{cases}$$

## D. Gaussian core

The Gaussian core model for the binary system is defined as<sup>12</sup>

$$u(r_{ij}) = \epsilon_{ij} \exp(-r_{ij}^2/\sigma_{ij}^2). \quad (3)$$

## E. Behavior at the origin

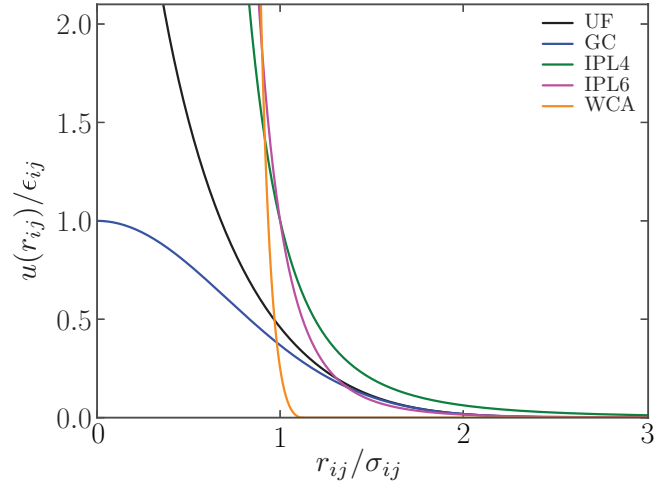


Figure S1. (Color online) Graphs of considered repulsive pair potentials.

The main difference between these models is their behavior near the origin, as can be seen in Fig. S1. The UF,

IPL4, IPL6 and WCA models all diverge at the origin, yet at different rates. Whereas the UF model diverges only logarithmically, the IPL4, IPL6 and WCA force fields diverge as  $r^{-4}$ ,  $r^{-6}$  and  $r^{-12}$ , respectively. The GC, on the other hand, does not diverge as  $r \rightarrow 0$ , reaching a constant value at zero slope.

## II. INSTABILITY WITH RESPECT TO COMPOSITION FLUCTUATIONS FOR THE UF MODEL

Depending of the magnitude of the inter-species energy scale, the random initial configuration for the UF model is unstable with respect to composition fluctuations, giving rise to the unmixing transition. This is illustrated in Fig. S2, which shows the mean energy obtained for 5000 random initial conditions as a function of composition at a reduced density  $\rho^* = 1$  for a number of different values for  $\epsilon_{AB}$ . For  $\epsilon_{AB} \lesssim 140$ , the energies are convex functions of the particle-type fraction, implying that the mixtures in these cases are stable. For  $\epsilon_{AB} \gtrsim 150$ , on the other hand, the curves have become concave for any com-

position, implying that mixtures in any proportion of *A* and *B* species are unstable<sup>13</sup>, giving rise to an unmixing transition.

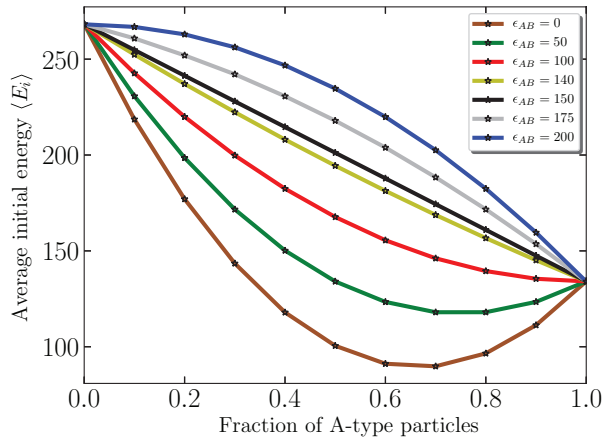


Figure S2. (Color online) Mean initial energy as a function of the *A*-particle fraction for different values of  $\epsilon_{AB}$ .

\* dekonig@ifi.unicamp.br

<sup>1</sup> G. Uhlenbeck and G. Ford, “Studies in statistical mechanics,” in *Series in physics*, v. 1, edited by J. de Boer and G. Uhlenbeck (North-Holland Publishing Company, 1962) Chap. The development of linear graphs with applications to the theory of the virial development of the properties of gases, p. 182.

<sup>2</sup> R. Paula Leite, R. Freitas, R. Azevedo, and M. de Koning, *J. Chem. Phys.* **145**, 194101 (2016).

<sup>3</sup> R. Paula Leite, P. A. Santos-Flórez, and M. de Koning, *Phys. Rev. E* **96**, 032115 (2017).

<sup>4</sup> R. Paula Leite and M. de Koning, *Comput. Mater. Sci.* **159**, 316 (2019).

<sup>5</sup> C. N. Likos, N. Hoffmann, H. Löwen, and A. A. Louis, *J. Phys.: Condens. Matter* **14**, 7681 (2002).

<sup>6</sup> C. N. Likos, H. Löwen, M. Watzlawek, B. Abbas, O. Jucknischke, J. Allgaier, and D. Richter, *Phys. Rev. Lett.* **80**, 4450 (1998).

<sup>7</sup> M. Watzlawek, C. N. Likos, and H. Löwen, *Phys. Rev. Lett.* **82**, 5289 (1999).

<sup>8</sup> A. Jusufi, M. Watzlawek, and H. Löwen, *Macromolecules* **32**, 4470 (1999).

<sup>9</sup> C. N. Likos, *Phys. Rep.* **348**, 267 (2001).

<sup>10</sup> S. Kambayashi and Y. Hiwatari, *Phys. Rev. A* **46**, 1014 (1992).

<sup>11</sup> J. D. Weeks, D. Chandler, and H. C. Andersen, *J. Chem. Phys.* **54**, 5237 (1971).

<sup>12</sup> F. H. Stillinger, *J. Chem. Phys.* **65**, 3968 (1976).

<sup>13</sup> D. A. Porter, K. E. Easterling, and M. Sherif, *Phase Transformations in Metals and Alloys (Revised Reprint)* (CRC Press, 2009).

<sup>14</sup> J. F. Panzarino and T. J. Rupert, *JOM* **66**, 417 (2014).

<sup>15</sup> A. Stukowski, *Model. Simul. Mater. Sci. Eng.* **18**, 015012 (2010).

<sup>16</sup> M. Newman, *Contemp. Phys.* **46**, 323 (2005).

<sup>17</sup> A. Clauset, C. Shalizi, and M. Newman, *SIAM Rev.* **51**, 661 (2009).